Simultaneous, coincident optical trapping and single-molecule fluorescence

Matthew J Lang[1,2,5,6], Polly M Fordyce[3,6], Anita M Engh[4], Keir C Neuman[1,2] & Steven M Block[1,2]

We constructed a microscope-based instrument capable of simultaneous, spatially coincident optical trapping and single-molecule fluorescence. The capabilities of this apparatus were demonstrated by studying the force-induced strand separation of a dye-labeled, 15-base-pair region of double-stranded DNA (dsDNA), with force applied either parallel ('unzipping' mode) or perpendicular ('shearing' mode) to the long axis of the region. Mechanical transitions corresponding to DNA hybrid rupture occurred simultaneously with discontinuous changes in the fluorescence emission. The rupture force was strongly dependent on the direction of applied force, indicating the existence of distinct unbinding pathways for the two force-loading modes. From the rupture force histograms, we determined the distance to the thermodynamic transition state and the thermal off rates in the absence of load for both processes.

Optical trapping (OT) and single-molecule fluorescence (SMF) are two powerful techniques that have facilitated much of the progress in the new field of single-molecule biophysics. OT can supply well-controlled loads that modify the free energy landscape of catalysis, translocation or folding and unfolding in macromolecules[1–3]. Position-detection systems incorporated into OT systems can report on the corresponding molecular displacements with nanometer sensitivity. OT instruments have been used to explore the molecular mechanics of biological motors[4], receptor-ligand binding[5–7] and biopolymer physics[8–10]. SMF approaches can probe length scales even smaller than those accessible to OT. Moreover, interactions between fluorophores—such as either fluorescence resonant energy transfer or fluorescence quenching—can report on the separation and relative orientations of domains within a macromolecule. Such interactions provide a spatial resolution of angstroms and can be used to monitor conformational changes occurring within proteins and nucleic acids, as well as to elucidate the dynamic and structural properties of biomolecules[11,12].

As powerful as the two techniques are individually, they each suffer from specific limitations that can be overcome by their application in concert. For example, it can be difficult to determine precisely where the load imposed by OT exerts its effect within a macromolecular complex. This location can be pinpointed by SMF, by attaching fluorescent probes to molecular subdomains and monitoring their subsequent motions. Conversely, the addition of OT to a SMF experiment can provide the ability to transport (or constrain) a macromolecule to an area optimized for fluorescence excitation, reducing the background light produced by neighboring fluorophores. In addition, molecules can be trapped and aligned before exposure to excitation light, increasing the useful fluorescence lifetime. Finally, correlations between fluorescence and mechanical signals can supply more information than can be obtained from either alone. For example, one can relate structural rearrangements occurring within molecules to their larger-scale motions to explore the mechanisms underlying conformational changes. Similarly, molecular binding events observed by fluorescence can be related to structural changes perturbed by load to determine the coupling between mechanical and biochemical cycles[13].

Marrying OT with SMF, however, poses technical challenges. The comparatively high light levels associated with the trapping and position-detection lasers can reduce fluorophore lifetimes through unwanted multiphoton bleaching of dyes or other destructive photochemical routes. Moreover, the lasers contribute light that can obscure the relatively weak fluorescence signal: a typical trap generates a photon flux roughly 15 orders of magnitude greater than that emitted by a single fluorophore. As a result, earlier attempts to combine OT with SMF did not achieve simultaneous, spatially coincident measurements. In previous work, these techniques were applied sequentially[13], or separately[14], by physically displacing the OT from the region of fluorescence excitation through a relatively large distance ($\sim$15 μm). Although these alternative approaches avoid photobleaching problems arising from the OT, each carries certain drawbacks. Sequential application precludes the possibility of temporally correlating the mechanical and fluorescence signals, whereas spatial separation imposes fairly severe restrictions on possible experimental geometries.

Here, we demonstrate simultaneous and spatially coincident OT and SMF by using an optical trap to separate the strands of individual DNA molecules labeled with fluorescent dye while monitoring both force and fluorescence. A preliminary report of this work has appeared[15]. We dissociated the duplex molecules using forces applied either perpendicular or parallel to the long axis

[1]Departments of Biological Sciences, [2]Applied Physics and [3]Physics, and [4]Graduate Program in Biophysics, Stanford University, Stanford, California 94305, USA. [5]Present address: Biological Engineering and Department of Mechanical Engineering, Massachusetts Institute of Technology, 77 Massachusetts Avenue, Cambridge, Massachusetts 02139-4307, USA. [6]These authors contributed equally to this work. Correspondence for materials should be addressed to S.M.B. (sblock@stanford.edu).

PUBLISHED ONLINE 21 OCTOBER 2004; DOI:10.1038/NMETH714

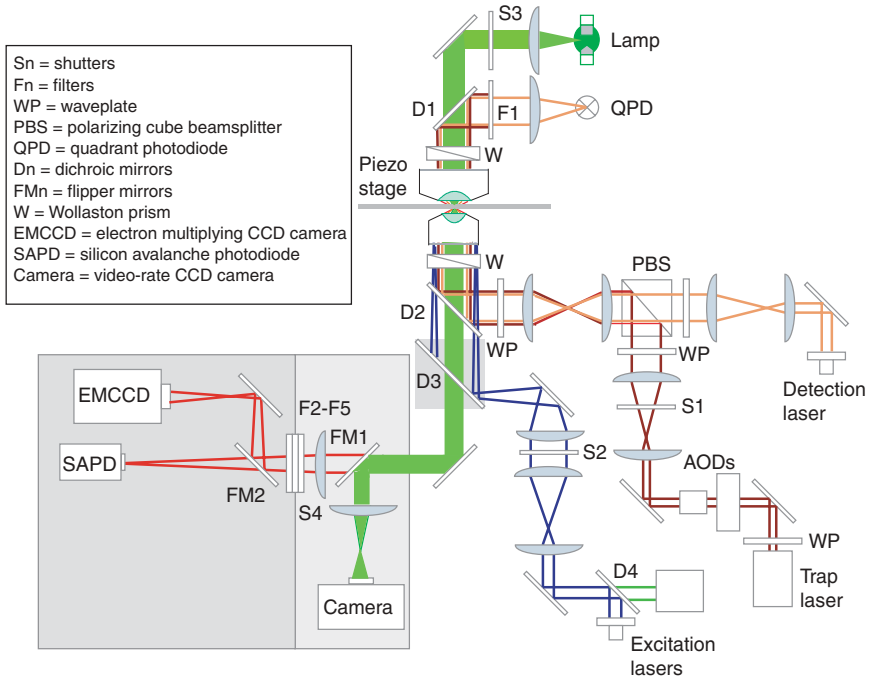

Figure 1 | Schematic optical layout of the instrument (not all components displayed). Light pathways are indicated for the mercury-arc transillumination (light green), trapping laser (dark red), position detection laser (orange), fluorescence excitation lasers (dark blue, green) and fluorescence emission (red). Some lasers are coupled with single mode fibers, as indicated. Photodetectors include a QPD for position sensing, a video-rate analog camera for general imaging, a digital EMCCD camera for SMF imaging, and a SAPD for photon counting. Electronic shutters provide automatic control of the trapping beam (S1), fluorescence excitation beam (S2), bright-field illumination (S3) and light entering the EMCCD/SAPD (S4). Multiple optical filters isolate the diode laser emission (F1) and block the trap, detection and excitation laser wavelengths before fluorescence detection (F2-F5). Flipper mirrors alternate between the video-rate camera and SMF subsystem (FM1) and choose the desired SMF detector (EMCCD camera or SAPD) (FM2).

of a short, 15-bp hybrid region (termed 'unzipping' or 'shearing' modes, respectively) and compiled histograms of the rupture forces required. These data constitute, to our knowledge, the first direct determination of the unzipping and shearing forces associated with the same DNA sequence. From the rupture force distributions, we extract zero-force parameters for the system, including the thermal off rate in the absence of load and the distance to the transition state along the reaction coordinate.

RESULTS

Instrument design

Our design aim was to combine OT and SMF without unduly compromising the capabilities of either technique. The instrument is based on a Nikon TE200 commercial inverted light microscope equipped with three lasers: one for trapping (1,064-nm Nd:YVO_4 laser; Spectra Physics); one for position detection (975-nm diode laser; Corning Lasertron); and one for fluorescence excitation (**Fig. 1**). The fluorescence source can be switched among a 514-nm argon-ion laser (Melles Griot Photonics), a 532-nm diode-pumped solid state frequency-doubled Nd:YAG laser (Coherent) and a 488-nm frequency-doubled diode laser (Blue Sky Research). The light from all lasers overlaps at the specimen. Fluorescence detection can be switched between a silicon avalanche photodiode (SAPD) for photon counting and an electron-multiplying CCD (EMCCD) camera for imaging.

Several design considerations allow OT and SMF to coexist. The wavelengths used for trapping and position detection were chosen to be well separated from those devoted to fluorescence excitation and emission, allowing the use of high-efficiency filters to reject the infrared trapping and detection light without compromising the fluorescence signal. High overall optical throughput in the infrared and optimization of beam diameter leads to improved trapping efficiency and detection sensitivity while minimizing the amount of laser power required, thereby reducing potentially damaging photon flux. Finally, computer automation of the instrument increases the usable lifetime of fluorophores by minimizing exposure to light during an experiment.

The instrumental components here differ from those described previously[15] in the following ways. First, we changed the wavelength of the position detection laser from 827 nm to 975 nm. Second, we incorporated two new diode-based fluorescence excitation lasers to illuminate a greater range of dyes. Third, we replaced the iCCD camera previously in use with an EMCCD camera. These modifications necessitated corresponding changes to the filters used to block collateral laser light.

Simultaneous force and fluorescence data

Figure 2 displays simultaneous single-molecule force and fluorescence traces recorded for four different experimental geometries, exerting either an unzipping or shearing force on a 15-bp hybridized region of DNA with tetramethylrhodamine (TAMRA) dyes conjugated at the various positions shown (**Fig. 3**). **Figure 2a** shows representative traces corresponding to an unzipping force, with the fluorophore linked to the long DNA strand. Before rupture the dye fluoresces normally. Upon rupture the fluorescence level decreases abruptly to an intermediate value as the bead-tethered fluorophore is pulled from the strongest region of evanescent wave excitation. The changes in fluorescence and force are concurrent. The fluorescence level decreases further to the background level when the computer, automatically detecting the rupture, instructs the trap to deflect the bead further from the excitation region.

To confirm that the drop in force corresponds to DNA strand dissociation and not to a breakage of the digoxygenin linkage holding the DNA-bead complex to the surface (or the like), we carried out control experiments with the fluorophore incorporated into the short 15-mer instead of the long strand (**Fig. 2b**). Here, fluorescence levels do not decrease concomitant with rupture, but instead bleach to background levels in a single step some variable time later ($\sim$10 s, on average). This demonstrates that a single dye

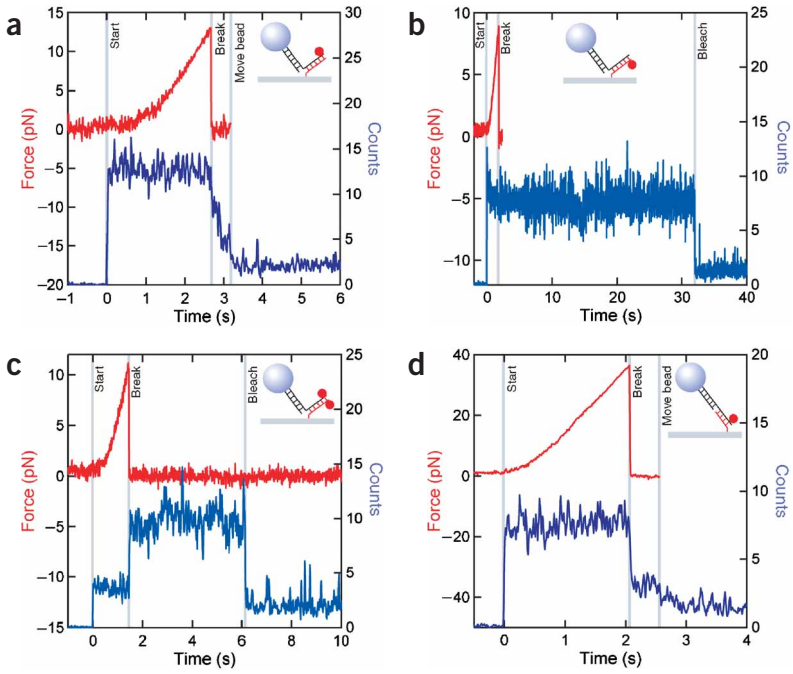

Figure 2 | Simultaneous traces of force (red) and photon counts (blue) recorded for four experimental geometries (insets). Fluorescence traces were smoothed with a 3-point boxcar filter. At the beginning of all traces, fluorescence excitation light was shuttered and DNA tether was pre-tensioned. At 'start' (vertical line, gray), excitation light was unshuttered and stage began to move at 100 nm/s. (**a**) Unzipping force applied to a complex with fluorophore attached to long strand. Rupture occurred at $t = 2.7$ s at $\sim$13 pN. Fluorescence levels decreased upon rupture, but remained above background levels as bead-tethered fluorophore diffused in and out of excitation. At 'move bead,' AODs moved bead with its tethered fluorophore away, reducing light to background levels. (**b**) Unzipping force applied to a complex with fluorophore attached to 15-mer. Rupture occurred at $t = 2$ s at $\sim$9 pN. Fluorophore photobleached in a single step at $t = 32$ s. Fluorescence noise after break and before bleaching reflects random motion of unloaded DNA tether carrying the fluorophore. (**c**) Unzipping force applied to a complex with fluorophores attached on complementary bases terminating the two strands. Rupture occurred at $t = 1.5$ s at $\sim$11 pN. The surface-bound dye unquenched at rupture, then bleached at $t = 6$ s. (**d**) Shearing force applied to a complex with fluorophore attached to the DNA long strand. Rupture occurred at $t = 2$ s at $\sim$35 pN. Noise in force trace is lower, due to increased tether stiffness associated with application of higher forces.

molecule is involved and that its fluorescence lifetime is acceptably long despite irradiation by the additional beams.

To further substantiate that rupture corresponds to DNA strand dissociation and to demonstrate the feasibility of using dye-pair quenching, we conducted unzipping experiments with TAMRA dyes conjugated to nucleotides on complementary bases, one located on the 3′-end of the 15-mer and the other on the 5′-end of the long strand (**Fig. 2c**). In these positions, the proximity of the dyes causes fluorescence quenching due to the formation of noncovalent dimers[16,17]. Before rupture, the low fluorescence level reflects the quenched emission. Upon rupture, the light level increases abruptly, corresponding to the mechanical separation of the two dyes, leaving an unquenched dye bound to the surface on the 15-mer. After several seconds, this dye photobleaches in a single step and the light drops to background levels. By combining the information supplied by the simultaneous trapping and fluorescence signals, the data show that discontinuities seen in the force traces correspond to true DNA strand separation, and not to the rupture of other noncovalent linkages in the system, something that is not straightforward to establish using either technique alone.

To test the dependence of rupture force on the direction of load application, we used the trap to apply a shearing force to the same DNA sequence, with the dye linked to the DNA long strand (**Fig. 2d**). As expected, a significantly higher force was required to separate the strands, and the fluorescence levels dropped concomitant with the mechanical rupture. In similar controls applying shearing forces to complexes with the dye on the 15-mer, the fluorescence level remained constant at rupture (data not shown). Here again, the combined OT and SMF signals establish that the bead and surface linkages do not break even at the higher forces used for shearing apart DNA.

To verify that TAMRA dyes fluoresced normally in the presence of all three lasers, we carried out an additional control experiment in which a DNA-tethered bead was moved back and forth in 20-nm increments by deflecting the trapping laser about a position directly above the bound fluorophore, under high trap power (**Fig. 4**). The fluorescence emission signal was uncorrelated with the movement of the trapping beam, and the dye photobleached in a single step.

DISCUSSION

Previous single-molecule studies have not determined unzipping and shearing forces for the same DNA sequence, but these have been estimated separately. One group measured the force required to unzip 48,000 bp of λ-phage DNA using a microneedle arrangement and reported unzipping forces on the order of 10–15 pN, depending on the local G-C content[18]. Another measured both shearing and unzipping forces using atomic force microscopy (AFM), first to shear apart a longer molecule of dsDNA and then to unzip the much shorter hairpins that formed in the resulting single-stranded DNA (ssDNA)[19]. They reported shearing forces of $\sim$150 pN for λ-DNA and unzipping forces between 9 and 20 pN for the hairpins. These values are not readily interpreted, however, owing to the unknown sequences and lengths of the hairpins that formed. Moreover, the DNA was nonspecifically bound to the AFM probe. An AFM study looked at the effect of varying duplex length and loading rate on shearing rupture forces between $\sim$20 and 60 pN for duplexes between 10 and 20 bp, but made no comparable unzipping measurements[20]. In another study, DNA molecules carrying single fluorophores were bound at either end to each of two derivatized, apposing microchip surfaces[21]. These surfaces were then mechanically separated, causing the DNA to rupture and leaving the fluorophore bound to either one surface or the other. By determining the fluorescence signal recovered from each surface

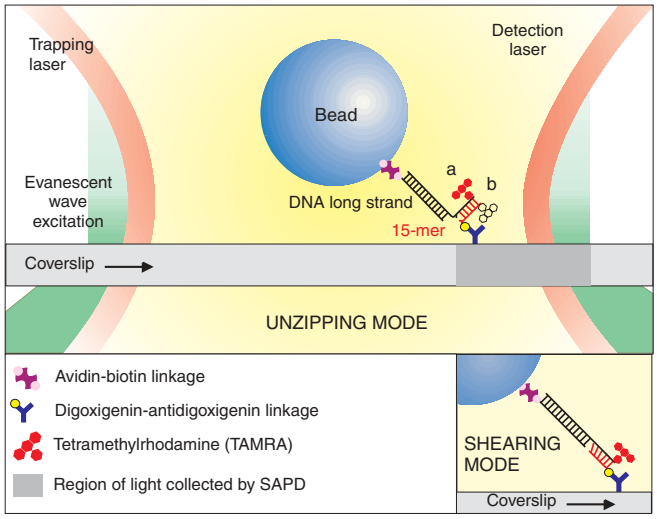

Figure 3 | Cartoon of the experimental geometry for both pulling geometries. A 500-nm polystyrene bead is tethered to coverglass surface by a 1,010-bp DNA molecule, consisting of a long segment (black) joined to a shorter 15-bp duplex region (red). The optical trap captures the bead and applies force to unzip or shear the short duplex. The long segment is attached to bead by means of a biotin-streptavidin linkage, and the 15-mer is attached to coverglass surface by means of a digoxygenin-antibody linkage. (a) Digoxygenin is attached to the 5′ end of the 15-mer for the unzipping mode. TAMRA dyes are attached to the end of DNA long strand (at position a) or to the 15-mer (at position b) for single fluorophore experiments, and attached at both positions for fluorescence unquenching experiments. (b) Digoxygenin is attached to 3′ end of the 15-mer for the shearing mode.

after strand separation, it is possible to compare the relative strengths of various DNA binding forces with respect to a reference signal from a control hybrid. This approach supplies rapid, qualitative information about the relative strengths of unzipping and shearing forces for small ensembles of molecules, but does not yield quantitative estimates.

Here, we have presented rupture-force distributions for unzipping and shearing geometries for the same 15-bp sequence. As anticipated, we found that significantly greater forces are required to separate the strands in shearing mode and that the variance of the shearing force distribution is wider than that of the unzipping force distribution (**Fig. 5**). The average unzipping rupture force was 10.3 ± 0.3 pN (s.e.m.; $n = 100$); the average shearing rupture force was 37.1 ± 1.1 pN (s.e.m.; $n = 83$). A stiffer optical trap was required to shear DNA complexes, increasing the loading rate to ~24 pN/s (as compared with ~11 pN/s for unzipping). Because of the known dependence of binding strength on force loading rate[22], this increased loading rate would be expected to produce a 9% increase in the critical breaking force, insufficient to account for the observed 3.6-fold difference. We directly fit the experimental rupture force distribution to the theoretical rupture probability density function for a single barrier transition to estimate the distance to the transition state and the thermal off rate in the absence of load[23] (see **Supplementary Note** online).

A fit to the unzipping force distribution gave $x = 1.9 \pm 0.2$ nm; this distance can be interpreted physically as the difference in distance measured between the 5′ and 3′ ends of the DNA duplex from the bound state to the transition state (see **Supplementary Note** online)[24]. Assuming an interphosphate distance of 0.42 nm for adjacent nucleotides in ssDNA under 10 pN load[25–27], we can relate x directly to the number of base pairs unzipped at transition: ~4.5 bp. Unzipping one base pair of dsDNA yields two ssDNA bases, suggesting that 2–3 bp of the dsDNA duplex are unzipped at transition, in reasonable agreement with the unzipping transition 'bubble' of ~4 bp predicted by nucleation theory[24], as well as the 3-bp nucleation bubble found for a poly(A)poly(U) acid[28]. For comparison, we computed the free energy predicted for hairpin unzipping under various loads (see **Supplementary Note** online).

A fit to the shearing force distribution gave $x = 0.49 \pm 0.05$ nm. In this case, the distance to the transition state represents the difference in the distance between the two 5′ ends of the DNA duplex between the bound state and the transition state (see **Supplementary Note** online). Modified wormlike chain models of dsDNA elasticity predict that adjacent base pairs remain separated by nearly their rest lengths (~0.34 nm) at the relatively low forces used in these experiments[29], so the difference in

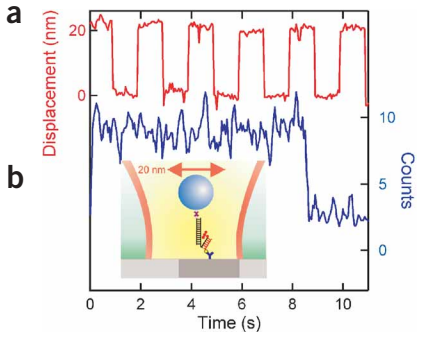

Figure 4 | Control trace demonstrating complete overlap of excitation, detection and trapping beams. (**a**) Bead is trapped and moved back and forth in 20-nm increments using AODs. QPD records bead position (red trace) while APD records photon counts (blue trace). Dye fluoresces normally, then photobleaches in a single step uncorrelated with trap movement. (**b**) Diagram of experimental geometry with bead trapped directly above the tether point, placing fluorophore within trap, detection and excitation beams.

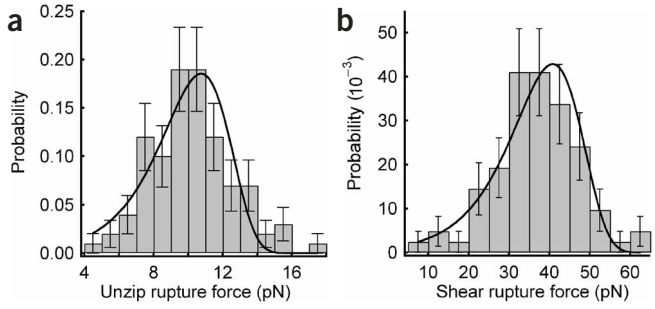

Figure 5 | Histograms of unbinding and shearing forces with fits to the probability distribution function for breakage force developed by Evans and Ritchie[28] (see **Supplementary Note** online). (**a**) Distribution of unzipping rupture forces; the average unzipping rupture force is 10.3 ± 0.5 pN (mean ± s.e.m.; full width half-maximum (FWHM) 5 pN, $n = 100$). (**b**) Distribution of shearing rupture forces; the average shearing rupture force is 37.1 ± 1.1 pN (s.e.m.; FWHM 15 pN, $n = 83$).

end-to-end separation provides a direct measure of the distance by which complementary strands are pulled out of register before rupture; the value for x suggests an axial displacement of 1–2 bp at transition.

The unloaded thermal off rates estimated from the fits to shearing and unzipping distributions agree within error ($\nu_0 = 0.03 \pm 0.01\ s^{-1}$ for unzipping versus $\nu_0 = 0.021 \pm 0.009\ s^{-1}$ for shearing). These values are three to five times lower than the off rate reported in a temperature-jump kinetics study ($0.1\ s^{-1}$) for a 16-bp DNA duplex (19% G-C content; pH 7.0; 200 mM Na^+)[30]. Thermal off rates are known to be a strong function of the G-C content, however, particularly for G-C pairs located at the opening of the helix[31], and this may account for some of the difference. We note that prior reports of thermal off rates estimated from mechanical data vary by over five orders of magnitude[20,24,31].

Finally, to confirm that the rupture forces we obtained were not systematically perturbed by the presence of conjugated TAMRA dyes, we compared the force distributions for complexes carrying either one or two fluorophores (see **Supplementary Note** online). For both shearing and unzipping modes, the one- and two-fluorophore distributions were statistically indistinguishable, suggesting that dyes conjugated to the terminal nucleotides contribute negligibly to duplex stability.

We have built an apparatus for simultaneous optical trapping and single-molecule fluorescence, and demonstrated its utility by measuring the forces required to unzip or shear a dye-labeled DNA duplex. We surmounted technical difficulties by separating the laser wavelengths devoted to trapping and position detection from those devoted to fluorescence; making judicious choices of dyes and filters; minimizing stray light and collateral illumination; and using extensive computer automation of the instrument to take optimal advantage of limited dye lifetimes. With minor modifications, the instrument reported here may be adapted to a variety of SMF modalities, including fluorescence resonant energy transfer (to monitor intramolecular distances) and polarized fluorescence excitation/emission (to monitor angular orientation). The ability to carry out fluorescence measurements on an optically trapped macromolecule should open up an entire range of biophysical experiments that were previously inaccessible. Applications suggested by this new technology include inserting pairs of fluorescent tags at target sites within macromolecules to probe the conformational changes responsible for features observed by force spectroscopy. In this fashion, individual domains can be monitored as changes in end-to-end separation are detected by optical trapping nanometry, revealing mechanisms responsible for conformational changes. This approach should be generally applicable to studies of protein (and nucleic acid) folding and unfolding and to a variety of binding studies. The same strategy may also be used, in principle, to detect more subtle rearrangements. For example, a fluorescent tag attached to a chaperonin complex might report its conformational state (say, the opening or closure of the lid) while an optical trap measures the force exerted on a bound protein. For research on molecular motors, this technology offers a direct way to observe coupling between the biochemical and mechanical cycles. In these experiments, simultaneous recording of motor motions detected with the optical trap and the binding and unbinding of fluorescent substrates can supply information about the relative timing of events.

METHODS

Instrument design. The optical layout is shown in **Figure 1**. Details of the microscope, OT and position detection subsystems are similar to those reported earlier[32]. The trapping and detection beams are coupled into the microscope above the epifluorescence filter cassette using a dichroic mirror that reflects the trapping and position detection wavelengths while transmitting visible light (>99% infrared reflectivity; ~90% transmission for 450–750 nm; Chroma Technology). The trapping laser can be adjusted to deliver 100–500 mW to the entrance pupil of the objective, depending on the desired trap stiffness. Trap laser throughput is maximized through the use of lenses and mirrors with antireflective infrared coatings, coated tellurium-dioxide acousto-optic deflector (AOD) crystals that transmit well in the infrared and half-waveplates to align the laser polarization with the axes of the Wollaston prisms within the microscope. The detection and fluorescence excitation lasers deliver 600 μW and 400 μW to 5 mW, respectively, measured at the same location.

Conventional methods of prism-based total internal reflection fluorescence (TIRF) were impractical in this system owing to spatial conflicts with the condenser lens used for position detection. Instead, fluorescence excitation light was coupled as an evanescent wave into the specimen by means of the objective (PlanApo 100×/∞/1.4-NA oil/IR, Nikon Biomedical; 61% transmission at 1,064 nm)[33–36]. This coupling yields a roughly elliptical excitation region in the specimen plane of area ~10 μm^2. An additional benefit of objective-side TIRF is that the illumination is immediately adjacent to the coverglass, where trap efficiency is also highest, minimizing the power required to trap (and eliminating the need for specialized, thin flow cells).

An EMCCD camera is used for visualization of fluorophores (iXon; Andor Technologies) and a SAPD is used for subsequent photon counting (EG&G Ortec); a motorized flipper mirror switches between these detectors. To enhance throughput and provide greater flexibility in the positions of the SAPD and EMCCD, we removed the microscope projection lens and replaced it with a singlet lens.

Efficient filters are necessary to allow the three laser beams to overlap in the specimen plane without drastically reducing fluorophore lifetimes or contributing excess noise from collateral illumination. To eliminate stray broadband diode emission from the detection laser, we isolated it with an ultra-narrow band-pass filter (~40% transmission over 972–978 nm) positioned in the detection beam path before the specimen plane (Andover). Additional filters were used to block collateral light downstream in the optical path: a glass filter (KG5, Schott Glass) for the trapping and detection wavelengths and Notch Plus holographic notch filters (Kaiser Optical) for all of the fluorescence excitation wavelengths. The KG5 filter transmits 80–90% of light over 350–600 nm, and has an optical density >5.0 beyond 900 nm. Each holographic notch filter has an optical density >6.0 within 10 nm of the center wavelength and transmits 80–90% of light outside this range. With the filters in place, the trapping and detection beams contribute no additional photon counts to background levels recorded by the SAPD. A beam block and standard barrier filters in the fluorescence filter cubes (Chroma Technology) extinguished the reflected TIRF light emerging from the objective.

The changes in laser wavelengths used in this apparatus necessitated changes to the filters used to block collateral illumination.

The barrier filter that isolates the detection wavelength was changed to 975 nm (Andover), and holographic notch filters (Kaiser Optical) were added to block each of the additional fluorescence excitation wavelengths. The ~300-μm diameter pinhole situated in front of the SAPD was removed to facilitate optical alignment; the instrument instead relies on the tiny size of the detector itself (~150 μm diameter) to ensure confocality with the image plane. This modification somewhat reduces the region in the specimen plane from which light is detected, to ~800 nm in diameter.

DNA duplex design. We constructed dye-labeled DNA tethers using the following scheme, allowing for the efficient substitution of different fluorophores and different surface-attachment chemistries. A 1,010-bp DNA duplex carrying a single-stranded, 15-bp 5′ overhang was attached to a 500-nm polystyrene bead at its blunt end (by means of a biotin-avidin linkage). The overhang was annealed to a complementary 15-bp synthetic oligonucleotide, anchored directly to the coverglass surface of a flow cell (by means of a digoxygenin-antibody linkage). The digoxygenin-linked base in the oligonucleotide can be placed at either end of the 15-mer, allowing force to be applied perpendicular or parallel to the axis of the short DNA hybrid for unzipping or shearing, respectively (**Fig. 3**). TAMRA dyes were conjugated to terminal nucleotides of the long (1,010 bp) strand, to the 15-mer, or to both strands. TAMRA dyes were used because the lifetimes of carbocyanine-based dyes are reduced in the presence of the trapping light, whereas rhodamine dye lifetimes remain comparatively unchanged (~10 s). A similar finding has recently been reported[37].

Details of the construction of the DNA duplexes, assembly of the bead-DNA complexes and preparation of flow cells are available in the **Supplementary Note** online.

Data collection and analysis. The apparatus was used to apply force to a bead-attached, fluorescently labeled DNA tether complex while concurrently recording bead displacement and photons emitted by the fluorophores. To do so, the bead was first optically trapped, then maintained in the trap as the piezoelectric stage carrying the flow cell was moved at constant speed, pulling the bead out of the trap center.

Measurement and calibration procedures were computer automated using custom software written in LabView (National Instruments). To begin each measurement, the detector beam was aligned with the center of the trap and the quadrant photodiode (QPD) as described[32]. Next, the tethered bead was centered in (x,y,z) coordinates based on measurements of the elastic extension of the DNA tether[38]. Rare tethers producing stretching curves with abnormal shapes or yielding incorrect contour lengths were discarded, eliminating beads with multiple tethers or non-specific attachments. Beads were positioned close to the coverglass surface to minimize movement in the z-direction. Each bead was then raster-scanned over the detection region to calibrate the QPD sensitivity[32]. During the centering and calibration procedures, the tether complex was exposed to light from the trapping and detection beams only, with the trap set to low power to minimize flux. After calibration, the stage moved the attachment point of the tether by 400 nm relative to the trap to remove slack from the tether.

At the start of data collection, the excitation shutter opens to allow fluorescence excitation light to reach the sample, and the stage pulls the bead out of the trap center, increasing the force on the complex until rupture. During data collection, the sample is exposed to light from all three lasers while the SAPD counts photons and the QPD collects position information at 200 Hz (filtered at 100 Hz). After rupture is detected, the AODs are used to move the trapped bead beyond the fluorescence excitation region to reduce background light emitted by trapped, dye-labeled bead-tether complexes diffusing in and out of the evanescent wave. In cases where the fluorophore remains fixed to the coverglass surface, the SAPD monitors the fluorescence signal until a photobleaching event occurs. Automated procedures limit the exposure of the dyes to unnecessary light.

Bead displacement from the trap center at the point of rupture is converted to a force in the x direction based on the measured trap stiffness, determined separately. The true force component along the direction of the tether is slightly greater than this force owing to the changing angle between the stretching DNA and the plane of the coverglass. This angular correction is small, and contributes no more than a 10% increase from the values reported here.

Note: Supplementary information is available on the Nature Methods website.

ACKNOWLEDGMENTS

We thank the entire Block lab for helpful discussions and J. Shaevitz for assistance with energy landscape calculations. This work was supported by grants to S.M.B. from the National Institutes of Health. P.M.F. acknowledges support from a National Science Foundation predoctoral fellowship and a Lieberman Award Fellowship; A.M.E. was supported by the Stanford Biophysics Training Grant from the National Institutes of Health; and M.J.L. was supported by a postdoctoral fellowship from the Jane Coffin Childs Foundation.

COMPETING INTERESTS STATEMENT

The authors declare that they have no competing financial interests.

Received 28 June; accepted 2 September 2004
Published online at http://www.nature.com/naturemethods/

1. Merkel, R., Nassoy, P., Leung, A., Ritchie, K. & Evans, E. Energy landscapes of receptor-ligand bonds explored with dynamic force spectroscopy. *Nature* **397**, 50–53 (1999).
2. Liphardt, J., Onoa, B., Smith, S.B., Tinoco, I. Jr. & Bustamante, C. Reversible unfolding of single RNA molecules by mechanical force. *Science* **292**, 733–737 (2001).
3. Onoa, B. *et al.* Identifying kinetic barriers to mechanical unfolding of the *T. thermophila* ribozyme. *Science* **299**, 1892–1895 (2003).
4. Schnitzer, M.J., Visscher, K. & Block, S.M. Force production by single kinesin motors. *Nat. Cell Biol.* **2**, 718–723 (2000).
5. Miyata, H., Yasuda, R. & Kinosita, K. Jr. Strength and lifetime of the bond between actin and skeletal muscle α-actinin studied with an optical trapping technique. *Biochim. Biophys. Acta* **1290**, 83–88 (1996).
6. Kawaguchi, K. & Ishiwata, S. Nucleotide-dependent single- to double-headed binding of kinesin. *Science* **291**, 667–669 (2001).
7. Nishizaka, T., Miyata, H., Yoshikawa, H., Ishiwata, S. & Kinosita, K. Jr. Unbinding force of a single motor molecule of muscle measured using optical tweezers. *Nature* **377**, 251–254 (1995).
8. Sun, Y.-L., Luo, Z.-P. & An, K.-N. Stretching short biopolymers using optical tweezers. *Biochem. Biophys. Res. Commun.* **286**, 826–830 (2001).
9. Wang, M.D., Yin, H., Landick, R., Gelles, J. & Block, S.M. Stretching DNA with optical tweezers. *Biophys. J.* **72**, 1335–1346 (1997).
10. Cui, Y. & Bustamante, C. Pulling a single chromatin fiber reveals the forces that maintain its higher-order structure. *Proc. Natl. Acad. Sci. USA* **97**, 127–132 (2000).
11. Forkey, J.N., Quinlan, M.E. & Goldman, Y.E. Protein structural dynamics by single-molecule fluorescence polarization. *Prog. Biophys. Mol. Biol.* **74**, 1–35 (2000).
12. Peterman, E.J., Sosa, H., Goldstein, L.S. & Moerner, W.E. Polarized fluorescence microscopy of individual and many kinesin motors bound to axonemal microtubules. *Biophys. J.* **81**, 2851–2863 (2001).

13. Funatsu, T. *et al.* Imaging and nano-manipulation of single biomolecules. *Biophys. Chem.* **68**, 63–72 (1997).
14. Ishijima, A. *et al.* Simultaneous observation of individual ATPase and mechanical events by a single myosin molecule during interaction with actin. *Cell* **92**, 161–171 (1998).
15. Lang, M.J., Fordyce, P.M. & Block, S.M. Combined optical trapping and single-molecule fluorescence. *J. Biol.* **2**, 6 (2003).
16. Blackman, M.J. *et al.* Structural and biochemical characterization of a fluorogenic rhodamine-labeled malarial protease substrate. *Biochemistry* **41**, 12244–12252 (2002).
17. Rosenfeld, S.S., Xing, J., Jefferson, G.M., Cheung, H.C. & King, P.H. Measuring kinesin's first step. *J. Biol. Chem.* **277**, 36731–36739 (2002).
18. Essevaz-Roulet, B., Bockelmann, U. & Heslot, F. Mechanical separation of the complementary strands of DNA. *Proc. Natl. Acad. Sci. USA* **94**, 11935–11940 (1997).
19. Rief, M., Clausen-Schaumann, H. & Gaub, H.E. Sequence-dependent mechanics of single DNA molecules. *Nat. Struct. Biol.* **6**, 346–349 (1999).
20. Strunz, T., Oroszlan, K., Schafer, R. & Guntherodt, H.J. Dynamic force spectroscopy of single DNA molecules. *Proc. Natl. Acad. Sci. USA* **96**, 11277–11282 (1999).
21. Albrecht, C. *et al.* DNA: a programmable force sensor. *Science* **301**, 367–370 (2003).
22. Evans, E. & Ritchie, K. Dynamic strength of molecular adhesion bonds. *Biophys. J.* **72**, 1541–1555 (1997).
23. Friedsam, C., Wehle, A.K., Kuhner, F. & Gaub, H.E. Dynamic single-molecule force spectroscopy: bond rupture analysis with variable spacer length. *J. Phys. Condens. Mat.* **15**, S1709–S1723 (2003).
24. Cocco, S., Monasson, R. & Marko, J.F. Force and kinetic barriers to initiation of DNA unzipping. *Phys. Rev. E* **65**, 041907–1–041907-23 (2002).
25. Williams, M.C., Wenner, J.R., Rouzina, I. & Bloomfield, V.A. Effect of pH on the overstretching transition of double-stranded DNA: evidence of force-induced DNA melting. *Biophys. J.* **80**, 874–881 (2001).
26. Bustamante, C., Smith, S.B., Liphardt, J. & Smith, D. Single-molecule studies of DNA mechanics. *Curr. Opin. Struct. Biol.* **10**, 279–285 (2000).
27. Cocco, S., Marko, J.F., Monasson, R., Sarkar, A. & Yan, J. Force-extension behavior of folding polymers. *Eur. Phys. J. E* **10**, 249–263 (2003).
28. Porschke, D. & Eigen, M. Co-operative non-enzymic base recognition. *J. Mol. Biol.* **62**, 361–381 (1971).
29. Bouchiat, C. *et al.* Estimating the persistence length of a worm-like chain molecule from force-extension measurements. *Biophys. J.* **76**, 409–413 (1999).
30. Turner, D.H., Sugimoto, N. & Frier, S.M. Thermodynamics and kinetics of base-pairing and of DNA and RNA self-assembly and helix coil transition. *Landolt-Bornstein New Ser. VII* **1c**, 201–227 (1990).
31. Porschke, D. Elementary steps of base recognition and helix-coil transitions in nucleic acids. *J. Biol. Biochem. Biophys.* **24**, 191–218 (1977).
32. Lang, M.J., Asbury, C.L., Shaevitz, J.W. & Block, S.M. An automated two-dimensional optical force clamp for single molecule studies. *Biophys. J.* **83**, 491–501 (2002).
33. Tokunaga, M., Kitamura, K., Saito, K., Iwane, A.H. & Yanagida, T. Single molecule imaging of fluorophores and enzymatic reactions achieved by objective-type total internal reflection fluorescence microscopy. *Biochem. Biophys. Res. Commun.* **235**, 47–53 (1997).
34. Moerner, W.E. & Fromm, D.P. Methods of single-molecule fluorescence spectroscopy. *Rev. Sci. Inst.* **74**, 3597–3619 (2003).
35. Axelrod, D., Burghardt, T.R. & Thompson, N.L. Total internal reflection fluorescence. *Annu. Rev. Biophys. Bioeng.* **13**, 247–268 (1984).
36. Axelrod, D. Total internal reflection fluorescence microscopy. *Methods Cell. Biol.* **30**, 245–268 (1989).
37. van Dijk, M.A., Kapitein, L.C., van Mameren, J., Schmidt, C.F. & Peterman, E.J.G. Combining optical trapping and single-molecule fluorescence spectroscopy: enhanced photobleaching of fluorophores. *J. Phys. Chem. B* **108**, 6479–6484 (2004).
38. Perkins, T.T., Dalal, R.V., Mitsis, P.G. & Block, S.M. Sequence-dependent pausing of single λ exonuclease molecules. *Science* **301**, 1914–1918 (2003).